Journal of Biomedical Optics 6(2), 141–150 (April 2001)

Threshold of fragmentation for ultrasonic contrast agents

James E. Chomas
Paul Dayton
Donovan May
Kathy Ferrara
University of California
Division of Biomedical Engineering
Davis, California 95616

Abstract. Ultrasound contrast agents are small microbubbles that can be readily destroyed with sufficient acoustic pressure, typically, at a frequency in the low megaHertz range. Microvascular flow rate may be estimated by destroying the contrast agent in a vascular bed, and estimating the rate of flow of contrast agents back into the vascular bed. Characterization of contrast agent destruction provides important information for the design of this technique. In this paper, high-speed optical observation of an ultrasound contrast agent during acoustic insonation is performed. The resting diameter is shown to be a significant parameter in the prediction of microbubble destruction, with smaller diameters typically correlated with destruction. Pressure, center frequency, and transmission phase are each shown to have a significant effect on the fragmentation threshold. A linear prediction for the fragmentation threshold as a function of pressure, when normalized by the resting diameter, has a rate of change of 300 kPa/μm for the range of pressures from 310 to 1200 kPa, and a two-cycle excitation pulse with a center frequency of 2.25 MHz. A linear prediction for the fragmentation threshold as a function of frequency, when normalized by the resting diameter, has a rate of change of –1.2 MHz/μm for a transmission pressure of 800 kPa, and a two-cycle excitation pulse with a range of frequencies from 1 to 5 MHz. [DOI: 10.1117/1.1352752]

Keywords: ultrasound; contrast agents; blood flow; optical observation; fragmentation.

Paper CARD-05 received Nov. 1, 2000; revised manuscript received Jan. 11, 2001; accepted for publication Jan. 11, 2001.

1 Introduction

Ultrasound contrast imaging can be used to estimate blood perfusion, based on a technique which involves intentional destruction of the agent. A destruction and wash-in technique has been proposed where contrast agents are first destroyed in a small sample volume, and then the flow rate for microbubbles entering the region is quantified using a nondestructive pulse sequence.[1] Imaging and contrast agent parameters each significantly affect the physical mechanism by which the microbubble is destroyed. Rapid destruction of the contrast agents can be accomplished by producing fragmentation, whereby the original microbubble is broken into many small fragments during one pulse of insonification. High-speed optical observation of contrast agent microbubbles, in conjunction with modeling techniques, is used to assess the effect of diameter, transmission pressure, frequency, pulse length, and phase on the onset of fragmentation.

Previous research on cavitation nucleated by a micron-sized gas microbubble focused on the cavitation threshold as a function of microbubble and imaging parameters. Fragmentation requires sufficiently large expansion followed by collapse of the microbubble, which concentrates enough energy to cause the microbubble to break apart. When the work done on the microbubble by the convergence of the surrounding liquid during collapse exceeds the dissipation of energy from the microbubble, the temperature and pressure inside the microbubble increase, leading to transient cavitation.[2]

The relative expansion of a microbubble, defined as the maximum radius R_{max} divided by the resting radius R_0, has been correlated with the cavitation threshold.[3,4] The physical mechanism that links the relative expansion to cavitation has been investigated in terms of the contributions of the inertial force and the pressure driving force during collapse.[5] Wall acceleration can be expressed as the sum of the acceleration due to the pressure force and the inertial force. For low-pressure insonation, the pressure force dominates and the wall acceleration reaches a peak magnitude which decreases as the bubble approaches its minimum radius. On the contrary, for high-pressure insonation, increasing amounts of kinetic energy are transferred to the contracting bubble when bubble collapse is driven by inertial forces. The acceleration mediated by inertial forces can become much larger in magnitude than that mediated by the pressure force, since it continues to increase as the bubble approaches its minimum radius. If the energy that is transferred during collapse is not sufficiently dissipated during one cycle, the bubble will become unstable and fragment. Therefore, conditions where the bubble acceleration is dominated by the inertial force are more likely to

Address all correspondence to James E. Chomas, Division of Biomedical Engineering, 1228 Bainer Hall, UC Davis, Davis, CA 95616. Tel: (530)754-9436; E-mail: jechomas@ucdavis.edu

1083-3668/2001/$15.00 © 2001 SPIE

fragment a bubble than conditions where the acceleration is dominated by the pressure force. The crossover between pressure-mediated collapse and collapse dominated by the inertial forces of the surrounding liquid depends on the relative expansion of the microbubble.[5] Relative expansion cavitation thresholds ranging from 2.32 to 3.463 have been predicted. The resting microbubble diameter and transmission center frequency are predicted to strongly affect the cavitation threshold pressure. Apfel and Holland show that a decreased center frequency decreases the pressure threshold and increases the resting diameter threshold (in this work, the cavitation threshold is defined by the pressure or resting diameter at which adiabatic collapse generates a temperature of 5000 K).[6] Previous work suggests that pulse length plays a role in cavitation due to rectified diffusion;[7] however, the pulse lengths studied in Ref. 7 are significantly larger than those studied in this work. Stability of the surface of a microbubble plays an important role in fragmentation. Rayleigh–Taylor instability of a spherical surface depends on both the wall velocity and wall acceleration.[8,9] When higher-order spherical harmonic amplitudes approach the size of the microbubble radius, the microbubble breaks up. Plesset and Mitchell predict that when the minimum microbubble radius decreases below one tenth of the maximum radius achieved by the microbubble, the microbubble will become violently unstable and fragment.[10]

In this work, optical techniques are used to observe a single microbubble while it is insonified with an acoustic pulse with varied pressure, frequency, pulse length, and phase. The optical system used in this work has been described previously.[11] The system generates seven two-dimensional images and a streak image. The streak image is captured by observing a vertical slice of the imaging field over time, much like an ultrasound M-mode image. If the slit is correctly aligned on the center of the microbubble, the streak image shows the diameter of the microbubble as a function of time. Key parameters, including the resting microbubble diameter, the relative expansion, and the timing of fragmentation, can be obtained with this technique. The temporal resolution of the system is 50 ns and the spatial resolution is approximately 200 nm. Motion of the microbubble wall is quantified according to the pixel size, with each pixel representing 120 nm. A logistic regression analysis is performed on the resulting data in order to quantify the relationship between imaging parameters, resting microbubble radius, and the onset of fragmentation.

A modified Rayleigh–Plesset equation is used to model the microbubble oscillations. The model accounts for the contrast agent shell, reradiation effects, and the van der Waals properties of the gas core;[11,12] however, the model assumes spherically symmetric oscillation. The bubble shell and gas parameters are specific to the contrast agent that is experimentally studied, and a rigorous explanation of the method by which these parameters were derived can be found in Refs. 11 and 12. The model results are compared to the experimental observations in order to understand the fragmentation threshold as it relates to relative expansion, predicted wall velocity, and predicted wall acceleration.

The paper is organized by first presenting experimental results with sections that focus on each imaging parameter. Statistical analysis of the experimentally observed fragmentation threshold is presented for pressure, frequency, and pulse length data. The experimental results are presented in conjunction with predictions for the relative expansion. The predicted wall velocity is calculated to determine the effect of the transmission phase. Discussion of the results and a conclusion follow the experimental and theoretical results.

Table 1 Transducer parameters.

Transducer	Center frequency (MHz)	6 dB Bandwidth (MHz)	Aperture size (in.)	Focal length (in.)
V311	10.5	7.5–13.6	0.5	2.07
V309	5.6	3.7–7.6	0.5	2.19
V305	2.4	1.6–3.3	0.75	2.34

2 Experimental Methods

All studies are performed with an experimental contrast agent MP1950 (Mallinckrodt, Inc., St. Louis, MO). The gas in the microbubble is C_4F_{10}, and it is encapsulated in a phospholipid shell. The agent is diluted in saline to approximately 1 sphere/μL. The diluted contrast agent solution is pumped through a 200 μm cellulose tube with a manual microinjector (Narishige, Inc., East Meadow, NY). The cellulose tube is positioned in the optical field of view of an inverted microscope (IX70, Olympus, Melville, NY). A 100× objective (Achroplan 100×, NA = 1.0, Zeiss, Thornwood, NY) and 1.6× zoom are used to obtain sufficient magnification. The cellulose tube is placed in a water bath chamber. In order to determine the effect of the transmission center frequency on the contrast agent, three transducers were utilized, each having a different center frequency. For a given experiment, one of the three spherically focused single piston transducers (V305, V309, or V311, Panametrics, Waltham, NY) is attached to one side of the water bath and the transducer is positioned confocally with the optical field of view and the cellulose tube. The center frequency, 6 dB bandwidth, focal length, and the aperture size for each transducer are described in Table 1. An arbitrary waveform generator (AWG 2021, Tektronix, Wilsonville, OR) generates the rf transmission waveform with arbitrary center frequency, pulse length, and amplitude. The signal is amplified with an rf amplifier (3100LA, ENI, Rochester, NY).

Optical data are captured with a high-speed camera (Imacon 468, DRS Hadland, Cupertino, CA). The camera captures seven individual two-dimensional (2D) images and a streak image. Light from a xenon flash illuminates the microsphere via a 1 mm fiber-optic cable. The light source and arbitrary wave-form generator are triggered by the high-speed camera. The individual 2D images are generated using a user-adjustable shutter duration. The minimum possible shutter duration is 10 ns, however, the images presented in this work are captured using a 50 ns shutter duration. A streak image is generated by capturing the image through a vertical slit over time, where the vertical slit is positioned at the horizontal center of the microbubble. All streak images presented in this paper are obtained with a temporal resolution of 10 ns.

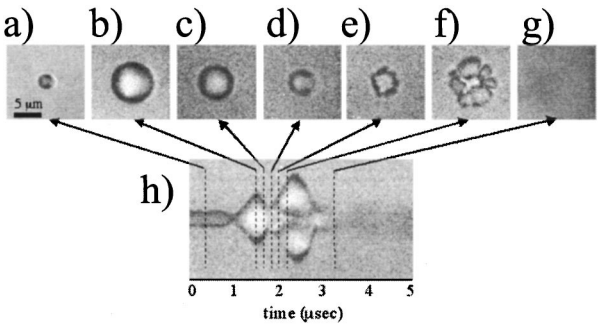

Fig. 1 Optical frame images and a streak image corresponding to the oscillation and fragmentation of a contrast agent microbubble, where fragmentation occurs during compression. The microbubble has a resting diameter of 3 μm, shown in (a). The streak image in (h) shows the diameter of the microbubble as a function of time, and the lines indicate the times at which the two-dimensional frame images in (a)–(g) were acquired relative to the streak image.

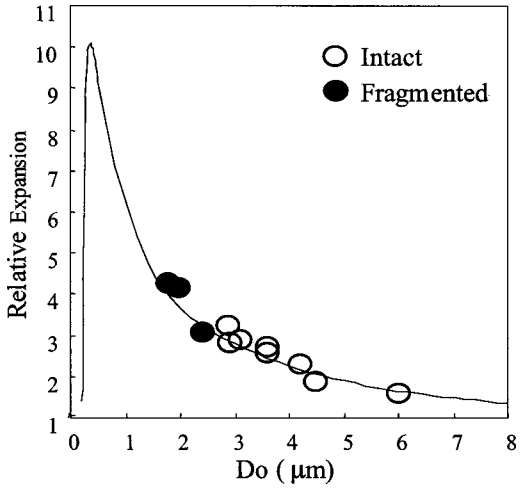

Fig. 2 Effect of resting diameter on relative expansion and fragmentation. Each microbubble is insonified with a one-cycle sinusoid, 2.25 MHz frequency, and 800 kPa peak negative pressure. Open circles represent microbubbles that are intact after insonation, closed circles represent microbubbles that are destroyed during insonation. The line is the predicted relative expansion.

Each transducer is calibrated while it is focused on the optical field of view with a needle hydrophone (PZT-Z44-0200 Specialty Engineering Associates, Soquel, CA) and a preamplifier (A17dB, Specialty Engineering Associates) connected to an oscilloscope. The tip of the needle hydrophone is positioned in the optical field of view.

The logistic regression analysis is performed using MATLAB, in conjunction with a statistical package known as GLMLAB (written by Dr. Peter Dunn, of the University of Southern Queensland). The link used in the analysis is logit, and a mean-deviance error measure is used.

3 Results

A total of 280 optical experiments were performed to observe the effects of microbubble resting diameter, transmission pressure, transmission center frequency, transmission phase, and pulse length on the relative expansion and fragmentation of contrast agent microbubbles. The optical system yields both a set of seven frames and a streak image for an individual experimental acquisition. Precise timing of the frames with respect to the streak allows visualization of the mechanism of the destruction of a microbubble during insonation. Subsets of data are generated by varying one imaging parameter while the others are held constant. Sample images for each subset of experiments are shown in order to offer a qualitative view of a contrast agent microbubble for a fixed resting microbubble diameter. The collection of images are quantitatively analyzed, with the results of this analysis presented graphically for each variable imaging parameter. For each parameter that is varied, open symbols represent microbubbles that remain intact and filled symbols represent microbubbles that are destroyed. Predicted relative expansion data generated by the model are shown with the experimental data. For wideband insonation studies, relative expansion is quantified by the maximum diameter before fragmentation, and the maximum typically occurs during the first expansion. For the pulse length study, the relative expansion is determined by the maximum expansion over all cycles, since fragmentation is occasionally observed to occur after many cycles even if the microbubble remained intact after the first cycle.

Figure 1 is a set of seven frames and a streak image of a microbubble undergoing Rayleigh–Taylor instability and resulting fragmentation. Figure 1(a) is the microbubble before insonation, with a resting diameter of 3 μm. The ultrasonic pulse is a two-cycle sinusoid, with a peak negative transmission pressure of 1.2 MPa. The microbubble is shown at the peak expansion of the first cycle in Figure 1(b), with a diameter of 10 μm. Figures 1(c) and 1(d) show the microbubble during compression after the first expansion, while it is still intact. Due to the high velocity experienced by the wall during the end of compression, Figure 1(d) appears blurred in both the frame and the streak. The microbubble fragments near peak compression, and is shown as a group of six fragments in Figures 1(e) and 1(f). Figure 1(g) shows the microbubble after the end of insonation, where three fragments are observed. A set of 2D images and a streak were acquired for each of the following sections to evaluate the phenomenon of fragmentation.

3.1 Microbubble Resting Diameter

The resting diameter profoundly affects the dynamics of an acoustically driven microbubble. While the effect of the resting microbubble diameter is apparent in all of the data that are collected, Figure 2 shows the effect of the resting microbubble diameter on the relative expansion for a fixed set of imaging parameters. Again, the open circles represent microbubbles that remain intact during insonation and the filled circles represent microbubbles that fragment during insonation. In Figure 2, the relative expansion is plotted versus resting diameter for the contrast agent insonified with a one-cycle sinusoid with peak negative pressure of 800 kPa and center frequency of 2.25 MHz. The acoustic pulse has a 180° phase, meaning rarefaction is followed by a large compressional half cycle. The relative expansion is inversely related to the resting diameter for the range of diameters that are tested. Fragmentation occurs more frequently for microbubbles with a small resting diameter rather than a large resting diameter, with a threshold size, below which fragmentation occurs, of

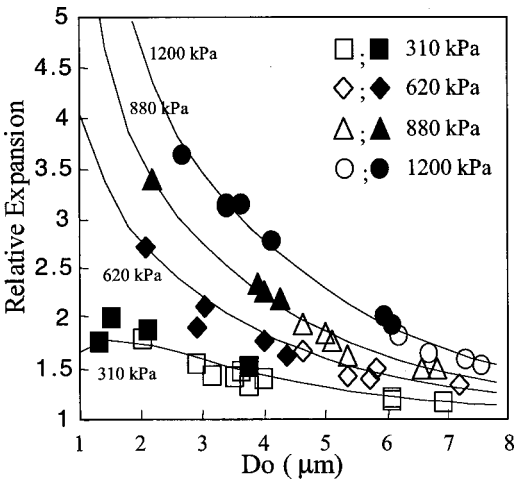

Fig. 3 Effect of pressure on relative expansion and fragmentation. Each microbubble is insonified with a two-cycle, 2.25 MHz sinusoid of varying peak negative pressure. Open circles represent microbubbles that are intact after insonation, closed circles represent microbubbles that are destroyed during insonation. Each line represents the predicted relative expansion. Relative expansion is calculated from the maximum diameter achieved before fragmentation.

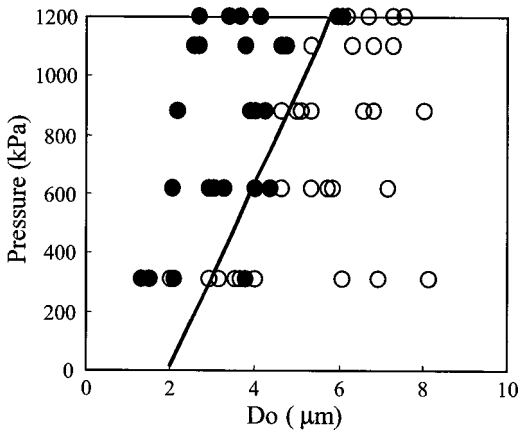

Fig. 4 Logistic analysis of the destruction threshold as a function of resting diameter and pressure. The threshold is represented by the line, open circles represent microbubbles that remained intact after insonation, and closed circles represent microbubbles that were destroyed. The predicted threshold is statistically significant in resting diameter ($p<0.0001$) and pressure ($p<0.0001$), and has a slope of 310 kPa/μm ($n=59$).

approximately 2.5 μm for these specific imaging conditions. The solid line represents the predicted relative expansion as a function of resting diameter. The model results are in agreement with the experimental results, showing an inverse relationship between the resting diameter and relative expansion for the range of resting diameters that are observed experimentally. It should be noted that for very small resting diameters, the relative expansion is predicted to decrease due to the increasing effect of surface tension, shown by the steep decrease in relative expansion a resting diameter smaller than 0.3 μm in diameter. Resting diameter will be included as a parameter in the studies of imaging parameters in the next sections.

3.2 Peak Negative Pressure

The transmission peak negative pressure is one factor in the thermal index (TI) and mechanical index (MI), two parameters that gauge the potential for dangerous bioeffects. Intuitively, increased transmission pressure should produce fragmentation; however, minimizing the transmission pressure with consistent fragmentation is desirable for clinical applications.

Figure 3 shows the effect of peak negative pressure and resting diameter on relative expansion and fragmentation of 59 microbubbles. All microbubbles are insonified with a two-cycle sinusoid with a center frequency of 2.25 MHz. The lines represent the predicted relative expansion as a function of resting diameter and transmission pressure. The predictions are in agreement with the experimental results, clearly showing that relative expansion increases with increasing peak negative pressure. For a fixed resting diameter of 3.75 μm, both theoretically predicted relative expansion and experimentally observed relative expansion increase from 1.5 for 310 kPa to 3.25 for 1200 kPa. For low transmission pressure, the relative expansion is independent of the resting diameter, while for insonation pressure greater than 310 kPa, the relative expansion increases exponentially with decreasing diameter. Increasing transmission pressure also increases the range of resting diameters for which microbubbles fragment, increasing the probability of fragmentation for large bubbles. For a fixed resting diameter of 3 μm, a microbubble insonified with a peak negative pressure of 310 kPa remains intact while a microbubble insonified with a pressure greater than 310 kPa fragments. Similarly, a microbubble with a resting diameter of 4.75 μm remains intact when insonified by 880 kPa or less but is destroyed when insonified with a peak negative pressure of 1200 kPa.

A resting diameter fragmentation threshold is calculated as a function of pressure using a binomial distribution logistic regression analysis ($n=59$). In Figure 4, the experimental data for fragmentation as a function of pressure and resting diameter are shown. Statistical analysis indicates that this threshold is significant for a range of resting diameters ($p<0.0001$) and pressures ($p<0.0001$). The threshold can be considered a resting diameter threshold, where below this resting diameter microbubbles are most likely to be destroyed. As a function of pressure, the resting diameter fragmentation threshold increases with increasing pressure. The predicted threshold is shown by the line, and is predicted to increase from 2.9 μm for 310 kPa to 5.8 μm for 1200 kPa. The threshold slope is 310 kPa/μm.

3.3 Center Frequency

The choice of center frequency of insonation determines the depth of penetration and the imaging resolution. In addition, the mechanical index, which indicates the probability of cavitation-induced bioeffects, is inversely proportional to the square root of the center frequency. A longer pressure rarefaction results in a larger maximum diameter and greater likelihood of instability. This is desirable when attempting to maximize the probability of microbubble fragmentation. However, the degraded resolution and the increased probability of bio-

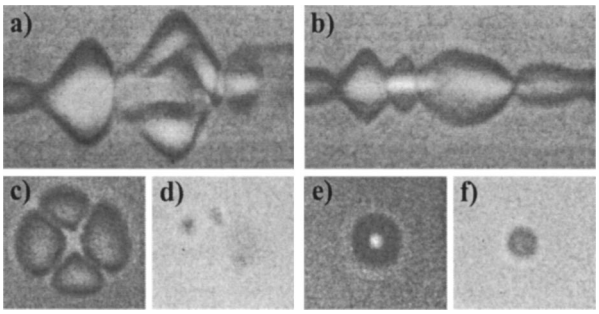

Fig. 5 Optical results of the effect of center frequency on microbubble oscillation and fragmentation. Each microbubble has a resting diameter of 3.6 μm and is insonified with a two-cycle sinusoid with a peak negative pressure of 800 kPa. The microbubble fragments when insonified with a center frequency of 1.5 MHz, shown in (a), (c), and (d). The streak image in (a) shows the fragments during compression after the first expansion. The second expansion is shown in (c), and fragments are observed after insonation in (d). Images (b), (e), and (f) show a microbubble insonified with 3.5 MHz, and clearly remains intact during the second expansion, shown in (e), and after insonation, shown in (f).

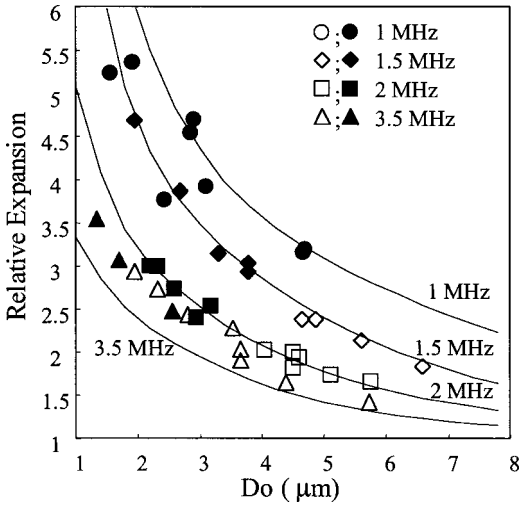

Fig. 6 Effect of frequency on relative expansion and fragmentation. Each microbubble is insonified with a two-cycle sinusoid with a peak negative pressure of 800 kPa and varying frequency. Open circles represent microbubbles that are intact after insonation, closed circles represent microbubbles that are destroyed during insonation. Each line represents the predicted relative expansion. Relative expansion is calculated from the maximum diameter achieved before fragmentation.

effects associated with lower frequencies make the desirable frequency as high as possible while maintaining the ability to destroy the microbubbles.

Figure 5 shows optical evidence of the effect of center frequency, with these two cases being representative of the 40 microbubbles that were studied. Figure 5(a) shows a streak image of a microbubble insonified with a 1.5 MHz center frequency while Figure 5(b) shows a microbubble insonified with a 3.5 MHz center frequency. The two microbubbles have the same resting diameter, 3.6 μm, and are each insonified by a two-cycle sine wave with peak negative pressure of 800 kPa. Clearly, the low-frequency insonation generates larger expansion, and the microbubble fragments after the first cycle. Figure 5(c) shows an image of the microbubble during the second expansion, where four fragments are observed, and Figure 5(d) shows the microbubble a long time after insonation. We note that the microbubble has fragmented with three fragments evident. Figure 5(e) shows the high-frequency case during the third expansion, and we note that the microbubble is intact. Figure 5(f) shows the same microbubble a long time after insonation, where the microbubble diameter is slightly decreased from 3.6 to 3.4 μm. Qualitatively, it is evident that a low-frequency pulse is more likely to fragment a microbubble than a high-frequency pulse, however, quantitative analysis of a set of microbubble diameters and frequencies is next performed to experimentally characterize the relationship between center frequency and fragmentation.

Figure 6 summarizes the effect of center frequency on relative expansion and fragmentation for 40 microbubbles. All microbubbles are insonified with a two-cycle sinusoid with a peak negative pressure of 800 kPa, and thus the time averaged intensity is not consistent. For all frequencies studied, the relative expansion ratio is inversely related to resting microbubble diameter. As observed in the images presented in Figure 5, decreased frequency produces an increase in the relative expansion ratio and occurrence of fragmentation for a fixed microbubble resting diameter and peak negative pressure. Similarly, the data presented in Figure 6 suggest a relationship between relative expansion ratio and occurrence of fragmentation over the entire data set. By grouping the data from all four frequencies ($n = 40$), 85% of microbubbles that exhibit a relative expansion ratio greater than 3 are destroyed while 10% of microbubbles that exhibit a relative expansion ratio less than 3 are destroyed.

The model prediction for relative expansion of microbubbles insonified with 1, 1.5, and 2.25 MHz is in agreement with the experimental data, again with an increase in relative expansion being observed for a decrease in center frequency. However, the predicted relative expansion for 3.5 MHz insonation is slightly less than that observed experimentally. The mean error in relative expansion is 13%, with the largest difference observed for microbubbles with a small resting diameter.

Figure 7 shows the maximum diameter achieved by a microbubble as a function of resting diameter and center frequency. The maximum diameter is quantified by measuring the largest diameter the microbubble achieves during insonation, which may include microbubble fragments in cases where the original microbubble is destroyed. These results may be useful in assessing the potential mechanical bioeffects of contrast-assisted ultrasound. For a given resting microbubble size, a decreased frequency results in an increased maximum diameter for the range of frequencies that are examined. The maximum diameter achieved is 8, 11, and 24 μm for 3.5, 2.25, and 1 MHz insonation, respectively. The predicted and experimentally observed maximum expansion for 3.5 MHz insonation is in agreement. This does not contradict the relative expansion data in Figure 6, where for 3.5 MHz insonation the model underestimates the relative expansion. The maximum expansion, as plotted in Figure 7, is achieved during the second cycle (and may be after fragmentation) while the relative expansion before fragmentation is plotted in

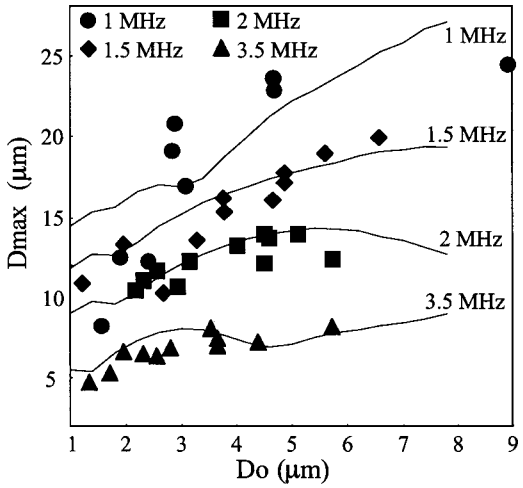

Fig. 7 Effect of frequency on the maximum diameter achieved by a microbubble. Markers represent the maximum diameter observed by a microbubble or its fragments, and the lines represent the predicted maximum expansion. Each microbubble is insonified with a two-cycle sinusoid with a peak negative pressure of 800 kPa.

Figure 6. The largest maximum diameter as a function of resting microbubble diameter is observed with 1 MHz insonation.

Logistical analysis of the effect of center frequency yields a resting diameter fragmentation threshold with a slope of approximately -1.2 MHz/μm. Logistical analysis is performed using optical data obtained from 85 microbubbles, insonified by a range of frequencies from 1 to 5 MHz. The optical data and predicted threshold are shown in Figure 8, again with open circles representing microbubbles that remain intact and closed circles representing microbubbles that fragmented. The line is the predicted threshold for fragmentation, which is significant in both resting diameter ($p<0.0001$) and center frequency ($p<0.0001$).

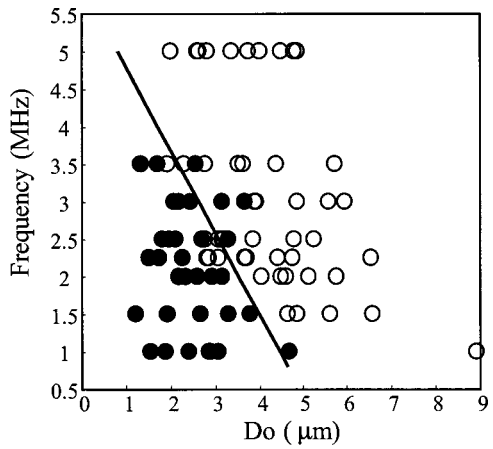

Fig. 8 Logistic analysis of the microbubble destruction threshold as a function of resting microbubble diameter and frequency. The threshold is represented by the line, open circles represent microbubbles that remained intact after insonation, and closed circles represent microbubbles that were destroyed. The predicted threshold is statistically significant in resting diameter ($p<0.0001$) and frequency ($p<0.0001$), and has a slope of -1.2 MHz/μm ($n=85$).

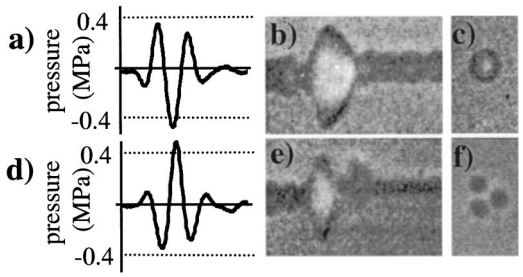

Fig. 9 Optical results of the effect of phase on microbubble oscillation and fragmentation. Each microbubble has a resting diameter of approximately 2.3 μm and is insonified with a 1.5-cycle sinusoid with an ISPPA of approximately 0.15 mW s/cm^2. The 0° waveform is shown by the solid line in (a), while the 180° waveform is shown by the solid line in (d). A phase of 0° generates a larger diameter during expansion, shown in the streak image of (b), but does not cause fragmentation, as observed by the intact microbubble after insonation in (c). A phase of 180° generates a smaller maximum diameter, shown in the streak in (e), however, the microbubble is observed to have fragmented, with the three fragments observed in (f).

3.4 Phase

The nonlinear effect of the phase of transmission on the received echo from ultrasound contrast agents has been pursued in a variety of imaging techniques.[12,13] The wall velocity and acceleration are dependent on phase, affecting the received echo amplitude and frequency. Therefore, it is reasonable to expect an effect of the phase of transmission on the onset of microbubble fragmentation.

Figure 9 provides direct visualization of a single microbubble that is insonified with a wideband pulse and the same peak pressure but different phase. Each microbubble is insonified with a 1 1/2-cycle sinusoid. The term ''0° phase'' describes the waveform shown as the solid line in Figure 9(a), with larger peak negative pressure than peak positive pressure, while the term ''180° phase,'' shown as the solid line in Figure 9(d), describes a wave with a larger peak positive pressure than peak negative pressure. The 180° insonation exhibits two rarefactional half cycles with rarefaction first, each with a peak pressure magnitude that is smaller than the compressional half cycle in the middle, while 0° insonation is comprised of two compressional half cycles with compression first. The peak negative pressure for the 0° phase transmission is 443 kPa, while the peak negative transmission pressure for the 180° phase transmission is 345 kPa. The integrated spatial peak pulse average (ISPPA) is approximately the same for each phase, being 0.154 mW s/cm^2 for the 0° phase and 0.147 mW s/cm^2 for the 180° phase.

Figure 9(b) is a streak image of microbubble insonified with 0° insonation, while Figure 9(e) is a streak image of a microbubble insonified with 180° insonation. The microbubble resting diameters are each 2.3 μm. The microbubble insonified with the 0° phase expands to a maximum diameter of 7.32 μm, larger than the expansion diameter of 5.73 μm observed with 180° insonation. However, the 0° pulse does not produce fragmentation, shown in Figure 9(c), while the 180° is shown to produce fragmentation, shown in Figure 9(f).

Data collected from optical experiments are shown in Figure 10, demonstrating the effect of the transmission phase of

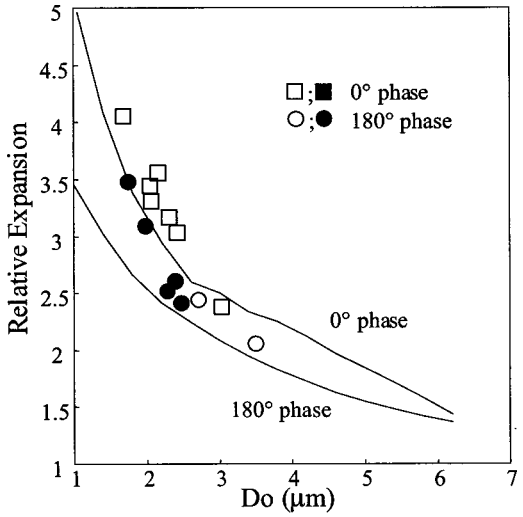

Fig. 10 Effect of phase on relative expansion and fragmentation. Open symbols represent microbubbles that remain intact while closed symbols represent microbubbles that fragment. The lines are predicted relative expansion, where relative expansion is calculated from the maximum diameter achieved before fragmentation. Each microbubble is insonified with a 1.5-cycle sinusoid with an ISSPA of 0.15 mW s/cm^2. Squares represent 0° insonation and circles represent 180° insonation.

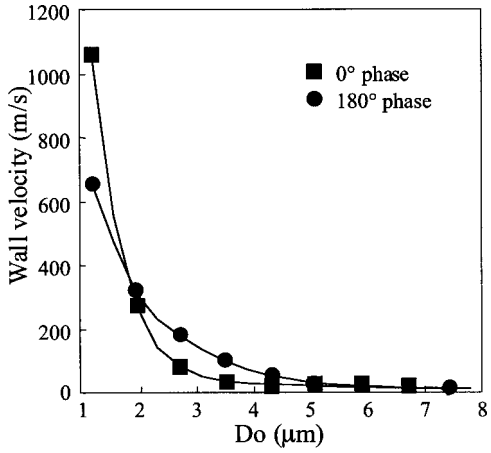

Fig. 11 Predicted wall velocity during compression as a function of phase and resting diameter. Diamonds represent the predicted wall velocity for 0° insonation, while squares represent the wall velocity for 180° insonation. In this figure, wall velocity during compression is defined by a positive value describing wall motion toward the microbubble center.

wideband insonation on the relative expansion and occurrence of fragmentation. For a fixed resting diameter, the 0° phase transmission produces larger relative expansion; however, a higher occurrence of fragmentation is observed for the 180° phase transmission than the 0° phase transmission. The resting diameter threshold for the 180° phase is approximately 2.75 μm, while the threshold is less than 2 μm for the 0° phase. The model results are shown for both phases of transmission, and the model predicts slightly lower relative expansion than observed experimentally, although both sets of data show the same trends. The larger relative expansion predicted and observed for 0° insonation is expected since the 0° pulse has a greater amplitude in the rarefactional half cycle than the compressional half cycle. However, the microbubbles that are destroyed are those insonified with a 180° phase pulse.

Model predictions for the microbubble wall velocity as a function of phase show that while 0° insonation produces a larger maximum microbubble diameter, 180° insonation produces a larger wall velocity over the range of microbubble resting diameters from 1.5 to 8 μm. The wall velocity as a function of microbubble resting diameter is shown in Figure 11, with the positive velocity during compression being defined by motion toward the microbubble center. For the case described in Figure 9, the microbubble that fragmented has a higher wall velocity than the microbubble that remained intact. Model results predict that for a 2.3 μm microbubble, 180° insonation is predicted to generate a wall velocity of 204 m/s, which is significantly higher than the wall velocity of 110 m/s generated by 0° insonation.

3.5 Pulse Length

Pulse length plays an important role in the spatial resolution of an ultrasound imaging system, with pulse length being inversely proportional to the imaging resolution. Increased pulse length can also increase the potential for thermal bioeffects, which is limited by the thermal index. Therefore, minimizing pulse length while maintaining the ability to destroy contrast agents is desired.

Images gathered from the study of pulse length are presented in Figure 12, showing optical data from four representative cases of the 121 microbubbles that were studied in this experimental subset. The images represent oscillations of microbubbles with a 5.1 μm resting diameter insonified by a 180° sine wave with a pressure of 400 kPa and center frequency of 2.25 MHz. Figures 12(a), 12(c), 12(e), and 12(g) indicate results with three-, five-, seven-, and ten-cycle insonation, respectively. Figures 12(b), 12(d), 12(f), and 12(h) are the full frame images acquired after insonation, providing

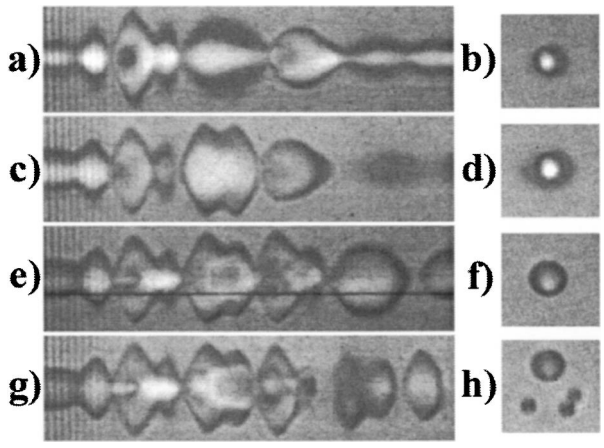

Fig. 12 Optical results of the effect of pulse length on microbubble oscillation and fragmentation. Each microbubble is approximately the same resting diameter, 5.1 μm, and is insonified by a 2.25 MHz sinusoid with a peak negative pressure of 400 kPa and varying pulse length. For each case, a streak image is shown and a full-frame image of the microbubble after insonation, shown for three cycles in (a) and (b), five cycles in (c) and (d), seven cycles in (e) and (f), and ten cycles in (g) and (h).

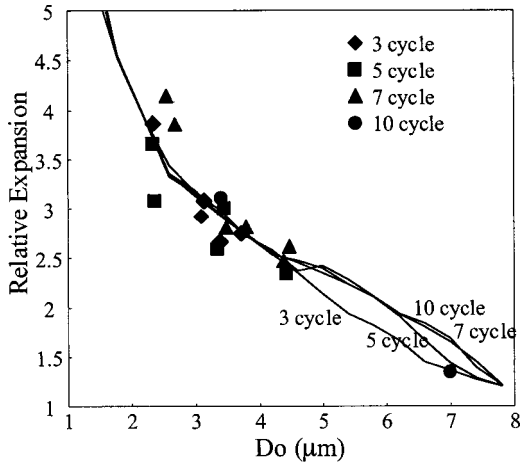

Fig. 13 Effect of pulse length on relative expansion. The symbols represent relative expansion and the lines are the predicted relative expansion, where relative expansion is calculated from the largest diameter observed during insonation, which differs from Figures 2, 3, 6, and 10 where wideband insonation was employed.

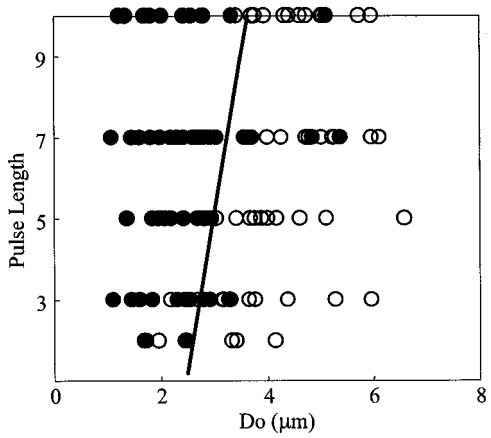

Fig. 14 Logistic analysis of the microbubble destruction threshold as a function of resting microbubble diameter and pulse length. The threshold is represented by the line, open circles represent microbubbles that remained intact after insonation, and closed circles represent microbubbles that were destroyed. The predicted threshold is statistically significant in resting microbubble diameter ($p < 0.0001$) and pulse length ($p < 0.02$), and has a slope of 8 cycles/μm ($n = 121$).

the opportunity to determine whether the microbubble is intact. As pulse length is increased, there is no observable increase in the relative expansion; however, the ten-cycle insonation results in the pinch-off of three fragments while the shorter pulse lengths do not appreciably affect the microbubble.

Figure 13 describes the effect of pulse length on the relative expansion as predicted by the model and observed experimentally. Long pulse length studies are difficult to perform with the streak camera due to the motion of the microbubble produced by the mechanisms of primary and secondary radiation force.[14] Furthermore, since the imaging system is only capable of generating seven full image frames, it is difficult to observe the exact time during the streak when the microbubble fragments, which is critical in the assessment of the relative expansion of the microbubble. Theoretically predicted relative expansion values are shown by lines while experimentally observed values are shown with markers. Relative expansion in the pulse length studies is defined by the maximum diameter over all cycles divided by the resting diameter. In the previous results showing the effect of pressure, frequency, and phase, relative expansion is determined by the maximum diameter before fragmentation, which is typically the maximum diameter during the first cycle. There is no significant increase in the predicted relative expansion for a resting diameter smaller than 4 μm; furthermore, no significant difference is observed experimentally. With a resting diameter greater than 4 μm, pulse lengths greater than three cycles are predicted to generate a slightly larger relative expansion compared to three cycles.

Figure 14 summarizes the effect of pulse length and resting diameter on fragmentation. These data were acquired by measuring the resting diameter and the final state of a microbubble. Occasionally, small fragments are observed near the original microbubble; however, unless the final diameter is less than 75% of the size of the original diameter, the microbubble is not considered to have fragmented. Possible mechanisms resulting in the other fragments are described in the discussion. Again, a logistic regression analysis is performed to predict the threshold for resting diameter and the results are shown in Figure 14 for the set of 121 microbubbles. The statistical analysis shows a small but significant effect of pulse length ($p < 0.02$), and a strong effect of resting diameter ($p < 0.0001$). The resting diameter threshold increases from 2.6 μm for a pulse length of two cycles to 3.6 μm for a pulse length of ten cycles.

4 Discussion

The optical results presented in this work offer insight into the mechanisms of rapid microbubble destruction; furthermore, destruction thresholds are predicted as a function of resting diameter and imaging parameters. The optical techniques used in acquiring images of contrast agent microbubbles bridge the gap between theoretical models of microbubbles and signal processing of the received echoes. The parameters that are readily available from the optical system are resting diameter, peak expansion diameter, final state of the microbubble, and a qualitative understanding of the underlying physical behavior of the acoustically driven microbubble.

An experimentally derived microbubble destruction threshold is useful in the design of a perfusion estimator based on a destruction and wash-in technique. In this method, microbubbles are continuously flowing through a vascularized region of interest, such as a tumor, and then destroyed using imaging parameters above the destruction threshold. The refresh of microbubbles is quantified by receiving echoes as microbubbles re-enter the region of interest. Key rheological parameters including blood flow velocity, total blood volume, and flow rate can be estimated using an indicator-dilution analysis. Contrast agents may improve perfusion estimates since the destruction of microbubbles can create a negative bolus in the region of interest without consideration of the transit of the bolus from the injection site to the imaging site.

In designing a destruction-based imaging technique, the optimal imaging conditions should maximize the destruction of microbubbles while maintaining resolution, depth of penetration, and safety constraints. Radiology applications favor the use of higher frequency and higher transmission pressure to maintain imaging resolution, since some radiological applications do not require large depth of penetration. In cardiology applications, where detection of gross perfusion defects is sufficient for some diagnoses, low frequency and pressure may be used in order to increase penetration with a safe mechanical index and consistent fragmentation. Narrow-size distribution would aid in the design of a destruction-based imaging technique. Small microbubbles are destroyed at lower MI and TI than large microbubbles, providing the ability to destroy microbubbles reproducibly while maintaining high frequency, and thus high resolution.

Microbubbles are observed to fragment during compression, just before or just after peak compression. High-speed streak camera studies are not able to resolve the exact timing of fragmentation; however, fragmentation occurs within 500 ps of peak compression.[11] Two possible mechanisms which may be responsible for the fragmentation of a microbubble are Rayleigh–Taylor instability and parametric instability, and these mechanisms may not be mutually exclusive. Rayleigh–Taylor instability, caused by a very large negative wall velocity and a positive wall acceleration, is most clearly observed in the study of the effect of the transmission phase. For a fixed pressure magnitude, microbubbles insonified with the 180° phase fragment, while those insonified with the 0° phase remain intact. Predictions of microbubble wall velocity and acceleration show that the 180° insonation generates significantly larger wall velocity and acceleration than the 0° phase, although the relative expansion produced by the 0° phase is larger. Since the pulse is wideband and a large wall velocity is produced, the mechanism is most likely to be Rayleigh–Taylor instability.

A second mechanism of microbubble destruction, parametric instability, is produced by shape instability that can occur during radial oscillation, especially when the microbubble is near a boundary. Parametric instability is caused in part by higher-order spherical harmonic oscillations growing without being sufficiently reduced by heat conduction, acoustic reradiation, shell viscosity, and other damping effects. This mechanism of destruction is apparent in the pulse length study, where the relative expansion, wall velocity, and wall acceleration remain nearly constant regardless of pulse length. However, a small but statistically significant increase in the destruction threshold is observed with increasing pulse length.

Nonspherical shape instability combined with increased wall velocity and acceleration may explain the profound effect of decreased resting diameter on the destruction threshold. In the experimental results concerning the effect of pressure, small microbubbles are observed to be destroyed by low-pressure insonation although they exhibit a lower relative expansion, predicted wall velocity, and wall acceleration than larger microbubbles that remain intact when insonified with higher pressure. This can be observed directly in Figure 3, where three microbubbles insonified with a transmission pressure of 310 kPa are destroyed. Theoretical calculations of wall velocity show that the largest predicted wall velocity for 310 kPa is -51 m/s, which is apparently sufficient to destroy very small microbubbles. In comparison, a wall velocity of -51 m/s is predicted to occur for microbubbles with diameters of approximately 5.8, 7, and 8 μm for 620, 880, and 1200 kPa. It is clear from Figure 3 that these microbubbles are well below the fragmentation threshold and were observed to be intact experimentally. These data suggest that small microbubbles are more likely to become unstable than large microbubbles given a fixed wall velocity and acceleration. The effect could be linked to the microbubble shell (which is assumed to be uniform with respect to microbubble size), the increase in radius of curvature that occurs with small microbubbles, or limitations of the model in predicting large and highly nonlinear microbubble oscillations.

Possible errors in the calibration of the experimental system make direct comparisons of the predicted thresholds difficult. Though hydrophone measurements are made frequently, the proximity of the microscope objective and fiber-optic light source to the acoustical focus may cause changes in the acoustic wave form. Perhaps the most likely candidate for error is in the hydrophone calibration itself. The needle hydrophone is too large to fit inside the water bath due to limitations in the size of the microscope stage, therefore, it was placed at an angle such that the tip of the hydrophone is in the optical focus. Variability in the angle of the hydrophone and its position relative to the microscope objective and fiber-optic light source may have caused changes in the hydrophone measurement. The error is largest in trying to compare the microbubble size threshold for 2.25 MHz and 800 kPa as calculated in the pressure study ($\sim$4.5 μm) and the frequency study ($\sim$3.5 μm).

Continued research with the goal of experimentally observing the mechanisms responsible for microbubble destruction will require higher temporal resolution to quantify wall velocity and acceleration; moreover, increased spatial resolution is required in order to sufficiently observe shape instabilities during the onset of fragmentation.

5 Conclusion

High-speed optical observation of contrast agent microbubbles provides the ability to experimentally quantify the threshold of destruction as a function of resting microbubble diameter and imaging parameters. Perhaps the most useful image is a streak image since it captures the diameter of a microbubble as a function of time. The experimental results in conjunction with model results suggest that for Rayleigh–Taylor-induced fragmentation, large wall velocity and acceleration are responsible for generating instability. Increased pressure increases wall velocity and acceleration, with the threshold size for destruction increasing from 2.9 μm for 310 kPa to 5.8 μm for 1200 kPa. The fragmentation threshold is inversely related to frequency, specifically, 1 μm for 5 MHz and 4.5 μm for 1 MHz, for 800 kPa insonation, respectively. Phase also affects the destruction threshold, with 180° insonation yielding larger wall velocity and acceleration, significantly increasing the probability of fragmentation for a fixed peak pressure magnitude and resting diameter. A slower mechanism of fragmentation is observed, which may be due to surface instabilities arising from nonspherical shape oscillations. In this case, wall velocity and acceleration may be lower than the Rayleigh–Taylor threshold, but over consecu-

tive cycles of insonation the pinch-off of microbubble fragments is observed. This mechanism is observed in evaluation of the effect of pulse length, where the maximum size for destruction with a pressure of 400 kPa is slightly increased from 2.6 μm for two cycles to 3.6 μm for ten cycles. The most significant factor determining the probability of fragmentation is resting diameter. A narrow size distribution in the range of 1–2 μm allows a range of imaging parameters to reproducibly destroy ultrasound contrast agents.

References

1. K. Wei, A. R. Jayaweera, S. Firoozan, A. Linka, D. M. Skyba, and S. Kaul, ''Quantification of myocardial blood flow with ultrasound-induced destruction of microbubbles administered as a constant venous infusion,'' *Circulation* **97**(5), 473–483 (1998).
2. T. G. Leighton, *The Acoustic Microbubble*, pp. 335–341, Academic, New York (1994).
3. R. E. Apfel, ''Acoustic Cavitation,'' in *Ultrasonics*, pp. 391–393, Academic, New York (1981).
4. R. E. Apfel, ''Possibility of microcavitation from diagnostic ultrasound,'' *IEEE Trans. Ultrason. Ferroelectr. Freq. Control* **33**(2), 139–142 (1986).
5. H. G. Flynn, ''Cavitation dynamics. II. Free pulsations and models for cavitation microbubbles,'' *J. Acoust. Soc. Am.* **58**, 1160–1170 (1975).
6. R. E. Apfel and Holland, ''Gauging the likelihood of cavitation from short-pulse, low duty cycle diagnostic ultrasound,'' *Ultrasound Med. Biol.* **17**(2), 179–185 (1991).
7. H. G. Flynn and C. C. Church, ''A mechanism for the generation of cavitation maxima by pulsed ultrasound,'' *J. Acoust. Soc. Am.* **76**(2), 505–512 (1984).
8. G. Birkhoff, ''Note on Taylor instability,'' *Quarterly Appl. Math.* **12**, 306–309 (1954).
9. G. Birkhoff, ''Stability of spherical microbubbles,'' *Quarterly Appl. Math.* **13**, 451–453 (1955).
10. M. S. Plesset and T. P. Mitchell, ''On the stability of the spherical shape of a vapor cavity in a liquid,'' *Quarterly Appl. Math.* **13**, 419–430 (1956).
11. J. E. Chomas, P. A. Dayton, D. May, J. Allen, A. Klibanov, and K. Ferrara, ''Optical observation of contrast agent destruction,'' *Appl. Phys. Lett.* **77**(7), 1056–1058 (2000).
12. K. Morgan, J. Allen, P. Dayton, J. Chomas, A. Klibanov, and K. Ferrara, ''Experimental and theoretical evaluation of microbubble behavior: The effect of transmitted phase and microbubble size,'' *IEEE Trans. Ultrason. Ferroelectr. Freq. Control* **47**(6), 1495–1509 (2000).
13. D. H. Simpson, Chien Ting Chin, and P. N. Burns, ''Pulse inversion Doppler: A new method for detecting nonlinear echoes from microbubble contrast agents,'' *IEEE Trans. Ultrason. Ferroelectr. Freq. Control* **46**(2), 372–382 (1999).
14. P. Dayton, K. Morgan, A. Klibanov, G. Brandenburger, K. Nightingale, and K. Ferrara, ''A preliminary evaluation of the effects of primary and secondary radiation forces on acoustic contrast agents,'' *IEEE Trans. Ultrason. Ferroelectr. Freq. Contr.* **44**(6), 1264–1277 (1997).